

Optimized Setup for 2D Convection Experiments in Thin Liquid Films

Michael Winkler¹ and Markus Abel^{2,1}

¹*University of Potsdam, Institute of Physics and Astronomy, 14476 Potsdam, Germany*

²*Ambrosys GmbH, 14473 Potsdam, Germany*

(Dated: September 11, 2018)

We present a novel experimental setup to investigate two-dimensional thermal convection in a freestanding thin liquid film. We develop a setup for the reproducible generation of freestanding thin liquid films. Such films can be produced in a controlled way on the scale of 5 to 1000 nanometers. Our primary goal is to investigate the statistics of reversals in Rayleigh-Bénard convection with varying aspect ratio; here numerical works are quite expensive and 3D experiments prohibitively complicated and costly. However, as well questions regarding the physics of liquid films under controlled conditions can be investigated, like surface forces, or stability under varying thermodynamical parameters. The thin liquid film has a well-defined and -chosen chemistry in order to fit our particular requirements, it has a thickness to area ratio of approximately 10^8 and is supported by a frame which is adjustable in height and width to vary the aspect ratio $\Gamma = 0.16$ to 10. The top and bottom frame elements can be set to specific temperature within $T = 15^\circ\text{C}$ to 55°C . The ambient parameters of the thin film are carefully controlled to achieve reproducible results and allow a comparison to experimental and numerical data.

PACS numbers: 47.52.+j,47.55.P-,68.15.+e,47.27.wj,47.55.pb,47.27.-i,82.70.Rr,47.51.+a

I. INTRODUCTION

Convection is of primordial importance with many applications from astrophysics to nanophysics, i.e. on the large scale¹ and on the small scale². Here, we present a two-dimensional analogue to the widely studied three-dimensional Rayleigh-Bénard convection cells: A vertically free-standing thin liquid film spanning across a metal frame is heated from below and cooled from above. The advantage of a two-dimensional setup is that the geometry can be varied with relative ease and the cost of construction and operation is far less compared to three-dimensional setups. However, these advantages are traded in for more complicated boundary conditions.

Our focus lies on the investigation of Rayleigh-Bénard convection, one paradigmatic system in hydrodynamics. It consists of fluid confined between a heat source with gravity acting parallel to the temperature gradient. It is widely used to study pattern formation and transitions between laminar and turbulent flow. In the last years, the question of reversals in Rayleigh-Bénard convection has been studied numerically and experimentally³⁻⁶. The setup is designed flexible in order to vary geometry and inflow boundary conditions, in particular the change of the flow characteristics with aspect ratio Γ (horizontal versus vertical dimension) and with temperature difference. Thereby, we cover fundamental and applied aspects, extending thin film experimental techniques to a very important non-equilibrium situation.

First steps towards experiments with stationary films and thermal driving have been reported, but the chemical composition and evaporation from the film have neither been controlled nor monitored⁷⁻⁹. One reason might be the relatively naive choice of chemicals (commercial detergents) which contain an ensemble of unknown surfactants and may contain anti-foaming agents which limit film stability. In contrast, many experiments with extremely well controlled chemistry and environment have been done on static thin films with a focus on the detailed understanding of interfacial physics, including surfactants and the chemical details of the liquid,¹⁰⁻¹³.

The presented measurement setup was designed with a precise control of the solution composition and ambient parameters in mind. As evaporation from the thin film, especially in heat driven convection scenarios can dramatically change the surface properties of a thin liquid film, a well-controlled experiment is needed.

It is possible to stably observe convection patterns for film thicknesses of 50 nm to 500 nm, over a long time. Consequently, the developed apparatus serves as a two-dimensional, well-controlled experiment using *stable, free-standing* thin liquid films to study two-dimensional

Rayleigh-Bénard convection. Typical Rayleigh numbers of 10^6 to 10^7 are reached with a centimeter size experiment.

Open questions concern the change of fluid properties with thickness, and the detailed influence of additional chemical forces (e.g. from surfactants), in comparison to classical fluid dynamics.

A. Thin Liquid Films

Thin film dynamics is governed by *gravitational*, *capillary* and *interfacial* forces. The drainage of thin films induced by the capillary pressure P_C is countered by interactions between the film surfaces. These interactions are combined in the disjoining pressure Π which acts perpendicular to the interfaces, thus balancing P_C . A quasistatic equilibrium is established when $P_C = \Pi$. The relevant interactions constituting Π are electrostatic, van der Waals (vdW), and steric forces^{14,15} and strongly depend on the distance between the interacting surfaces.

Whereas films on substrates are established in industry and research¹⁶, freestanding thin liquid films (hereafter TLFs) still provide a challenge in experiments and theory alike. Consequently, the study of TLFs is central to many current scientific activities, e.g.^{10,17-21}. We contribute by presenting a novel experimental setup to analyze convection in *vertically oriented, freestanding, thermally forced, non-equilibrium* TLFs.

As a result of the force balance, two stable equilibria may occur, depending on the chemical composition of bulk solution and chosen surface active agents (surfactants): Common Black Films (CBF) with a thickness of more than 10 nm are formed when electrostatic interactions balance the dominant van der Waals force, and, of course, gravity and capillarity^{15,22}; Newton Black Films (NBF) are stable with a thickness of less than 10 nm, due to repulsive short range steric forces^{23,24}. Depending on the chemical composition of the liquid the film will reach a NBF or CBF^{10,11}. In order to distinguish these cases it is essential to have well controlled experimental conditions: filtered, deionized water, pure surfactants and control over the ambient parameters (temperature and humidity).

For the non-equilibrium dynamical behaviour, studies have so far focused on the role of gravitational or capillary forces in undisturbed, freestanding TLFs^{11,25}. The effect of additional forces has been studied by a few authors, mostly for micrometer-thick systems^{26,27}. The formation of TLFs, aided by thermal forcing is an open issue on the nanoscale. For the most part of the

presented convection experiments the TLF will be in a quasi-steady but transient state. The convection prevents stratification, therefore the TLF does not reach its equilibrium thickness (CBF or NBF): the slow, gravity driven thinning is counteracted and a more uniform thickness is maintained. In this quasi-steady state convection is vigorous and can last indefinitely without the formation of an equilibrium phase layer. Additionally, the convection can be triggered after the TLF has reached its equilibrium NBF state so that forced convection in a sub 50 nm TLF can be observed. To our knowledge our setup is the first to make this observation possible. As the CBF or NBF show almost no reflection of (visible) light due to the particular interference conditions (the film can be much thinner than visible light), data acquisition and analysis is challenging.

The driving mechanism in this setup is a temperature gradient antiparallel to gravity which results in a buoyancy-driven convection, analogue to classic Rayleigh-Bénard convection. Please note that no Marangoni type flows are present in this setup ($Ma \simeq 0$). The TLF is bound by the frame, such that no conventional Marangoni effect occurs, since there is no free interface and consequently no thermocapillary effect occurs. However, there is an interface with the holding frame, subject to no-slip boundary conditions, which hinders any tangential flow. More heuristically, a Marangoni effect would drive a flow orthogonal to the vertically oriented surface. We, however observe a flow in the plane of the film, i.e., transversal to the surface. Additionally, the surface is mobile and therefore no surfactant concentration gradients arise which could lead to a Marangoni flow^{28,29}. No surface stresses can arise and the surface tension is constant³⁰ at $\sigma = 34 \cdot 10^{-3} \text{ N/m}$.

B. Rayleigh-Bénard-Convection in Thin Liquid Films

One of the long-standing, very important questions in convection problems concerns the understanding of the convective-to-conductive heat transport, measured by the Nusselt number, $Nu = Nu(Ra, Pr, \Gamma)$, and of the momentum transport, characterized by the Reynolds number, $Re = Re(Ra, Pr, \Gamma)$, where Γ denotes the aspect ratio of the container. The scaling of $Nu(Ra)$, $Re(Ra)$ has been studied, mainly in water and air, few for liquid metals. The corresponding range of Prandtl numbers is relatively limited. Experimental studies on the aspect ratio, Γ , exist, are however cost intensive, e.g. for the "barrel of Ilmenau"³¹, where a variation of $0 < \Gamma \lesssim 1$ is possible by controlling the cool top of a cylindrical vessel^{32,33}.

Under certain conditions, a flow develops a large-scale circulation (LSC). It is observed experimentally and numerically in 3D and 2D that this LSC breaks down and/or reverts in a regular or irregular way, depending on Ra and geometry^{3,34–38}. Recent 2D numerical studies of Lohse et al. indicate that the dynamics of reversals strongly depends on Γ^3 .

In contrast to 3D convection experiments, there is relatively little done *experimentally* on 2D, or quasi-2D systems. Initial convection studies of foam films were carried out by Mysels³⁹, later by Couder⁴⁰. A theoretical framework was established by Chomaz⁴¹ and Bruinsma⁴². Typically, free-standing TLFs are employed as fluid systems, where a collapse of the film is prevented by repumping liquid in order to compensate for losses due to evaporation, and of course gravitational flow downwards⁴³. This results in relatively uncontrolled boundary conditions, since the free surface can vary in thickness and can even develop instabilities (ripples, etc.). However, the system is well suited for experiments on 2D turbulence, because for Reynolds numbers up to at least 10^8 the thickness is well below the Kolmogorov length, which marks the scale above which no turbulence occurs, and dissipation dominates the momentum transfer⁴⁴. In 2D, the momentum is transferred from small to large scales by the so-called "inverse cascade" in contrast to 3D, where the opposite is observed as the "direct cascade"^{44–46}. In extremely large TLFs (with heights of several meters) information about the inverse cascade is observed experimentally by particle imaging and laser doppler velocimetry. A well explored topic is the evolution of grid turbulence with seeded sub-micron particles^{7,47–50}.

For a two-dimensional TLF, one can assume an effective decoupling of buoyancy-caused advection and surface-related relaxation due to disjoining and capillary pressure. Of course, in a complete, 3D description basically all forces are coupled. For very small length scales, a molecular description is necessary, however the hydrodynamic approximation holds well down to a few molecular layers. These issues and further details can be read in⁵¹, where, however, mainly fluid confined by solid walls are considered. More fundamental discussion is given in^{35,52–54}. It is expected that the scales considered here (> 5 nm) are sufficiently described by hydrodynamic equations. This assumption is not completely unreasonable as $Ra \sim 10^7$ and thus other forces are smaller by orders of magnitude.

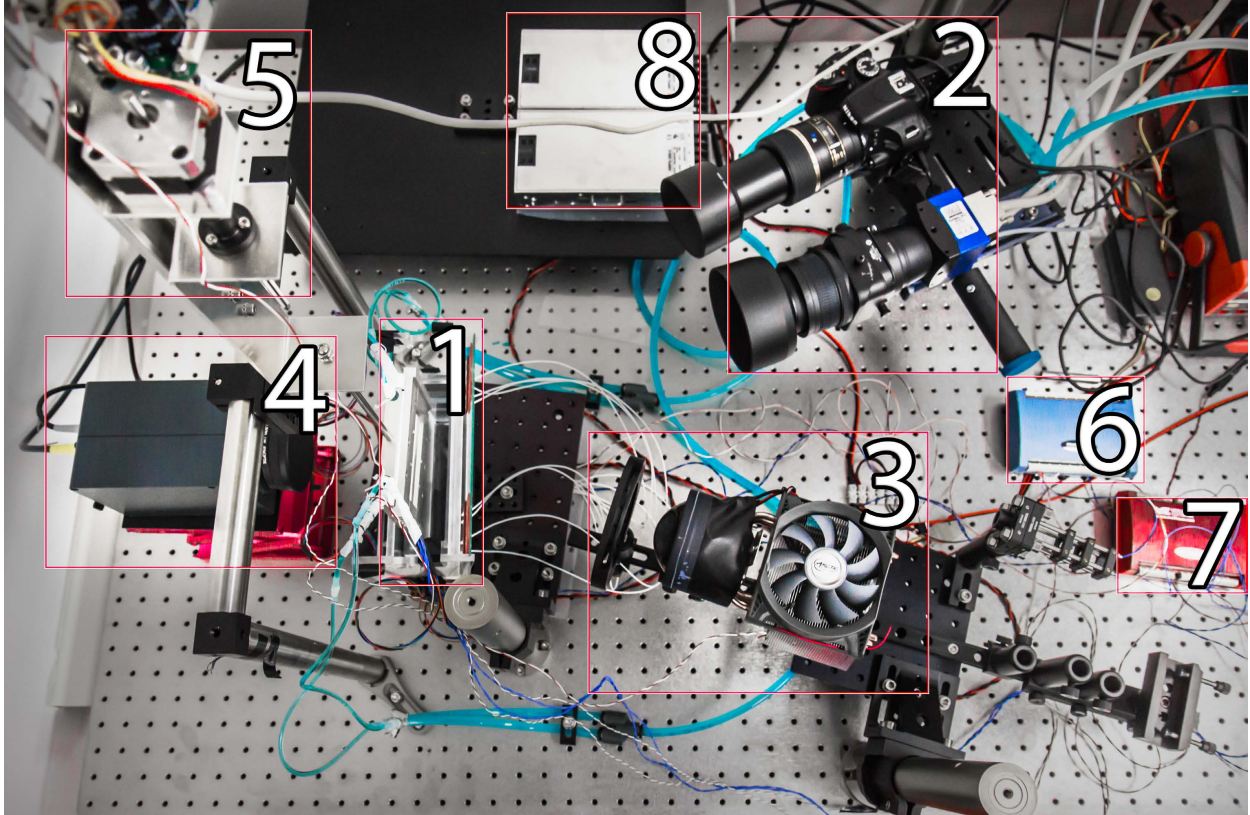


Figure 1: Measurement setup - top view. (1) frame assembly, (2) video and still frame cameras, (3) lamp, (4) IR camera, (5) motor assembly, (6) voltage generator, (7) temperature measurement unit, (8) power supplies. Heat exchanger is not shown. top and back lid of the measurement chamber where removed for better visibility.

II. SYSTEM DESCRIPTION

Figure 1 is a photograph of the complete experimental setup. The details of the system will be described in section III and IV.

A. Key features

Our setup is focused on the study of the influence of the aspect ratio on the convection pattern by a frame, holding the TLF, which can be varied in width and height independently. A closed measurement chamber meets the requirements for controlled ambient parameters. The temperature control units for a temperature gradient similar to classic Rayleigh-Bénard-Convection. The liquid film is heated at the bottom and cooled at the top by an array of thermo-electric

couples (TEC) which is built into the frame which supports the freestanding thin liquid film. In table I the system parameters are summarized and additionally the feasible Rayleigh and Prandtl numbers are shown in figure 2. The main features of the setup are:

- The aspect ratio Γ of the film is variable with a film height range of $h_{film} = 5 - 30$ mm and film width range of $w_{film} = 5 - 50$ mm. This covers an aspect ratio of $\Gamma = 0.16 - 10$.
- The Rayleigh number can be varied in the range of $R_a = 10^6$ to 10^7 by adjusting the temperature gradient, cf. Fig 2(a).
- The Prandtl number can be adjusted by varying the viscosity, respectively glycerin content, cf. Fig. 2(b).
- The case is completely transparent to allow optical measurements of the film. The rear panel of the case can be exchanged with a panel containing a Germanium window to allow thermal imaging with an infrared camera.
- The front window is angled downwards with respect to the TLF-plane to prevent reflection from the light source off the front glass into the camera to enhance imaging contrast.
- The Temperature of the horizontal lower and upper frame parts are precisely controlled by an array of thermoelectric couplers (TECs).
- The front window can be heated to avoid condensation and regulate ambient temperature.
- The humidity inside the measurement cell is measured and controlled by evaporating water from a separate chamber.
- The pressure is set by ambient pressure, but can be controlled by sealing the setup. We do not use this feature, though.

B. Measurement Chamber

The measurement cell is composed of four parts, displayed in an explosion view rendering in figure 3. The container (1) has a rectangular cavity which fits the solution reservoir (2). Additionally, there is a U-shaped reservoir in the container with two resistive heating elements built in. This reservoir is filled with deionized water and used to regulate the humidity inside the chamber via an automated control loop using a humidity sensor. The frame assembly (3) fits

Area	A	$0.025 - 1.5 \cdot 10^{-6} \text{ m}^2$
Density	ρ	$1019 - 1080 \text{ g/m}^3$
Dynamic viscosity	μ	$0.7 - 3.7 \text{ Ns/m}^2$
Kinematic viscosity	ν	$0.7 - 3.1 \cdot 10^{-6} \text{ m}^2/\text{s}$
Mean velocity	u	approx. $2 \cdot 10^{-2} \text{ m/s}$
Raleigh number	Ra	$0.37 - 1.62 \cdot 10^7$
Prandtl number	Pr	$12 - 38$
Specific molar heat capacity	c_p	$207 - 254 \text{ J/molK}$
Surface tension	σ	$34 \cdot 10^{-3} \text{ N/m}$
Thermal diffusivity	α_{th}	$5.8 - 8.0 \cdot 10^{-8} \text{ m}^2/\text{s}$
Thermal conductivity	κ_{th}	$0.49 - 0.60 \text{ W/m}\cdot\text{K}$
Thermal exp. coefficient (vol.)	β	$255 - 362 \cdot 10^{-6} \text{ K}^{-1}$
Hamaker constant	C_H	$0.5 \cdot 10^{-20} \text{ J}$

Table I: Parameters of the experiment.

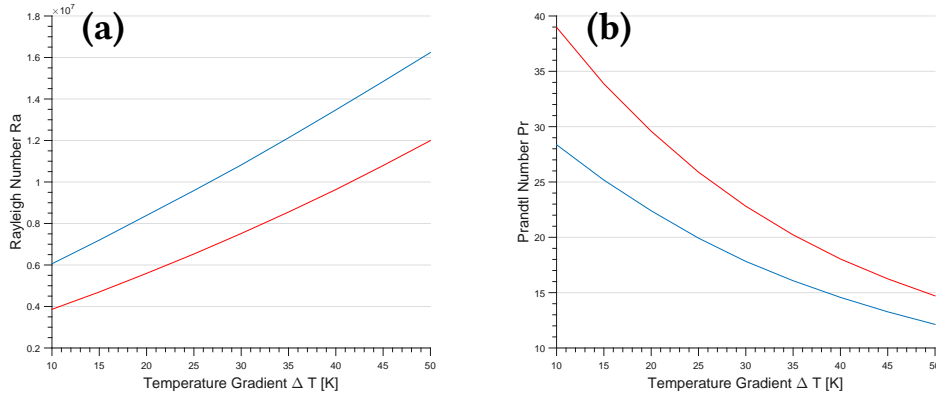


Figure 2: (a) Rayleigh number and (b) Prandtl number scaling with available temperature and viscosity ranges for 10%_{vol} (blue) and 25%_{vol} (red) glycerol.

into the film solution reservoir (2) in which it can be submerged and pulled out by an automated motorized control. The top enclosure of the setup (4) sits on top of the bottom reservoir and shields the thin liquid film thus allowing for a precisely controlled atmosphere (temperature and humidity) inside the measurement cell.

The dimensions of the measurement cell are based on the frame (3) dimensions 85 - 90 - 25 mm (width - height - depth). Therefore the outer dimensions of the complete measurement cell are 190 - 170 - 100 mm (width - height - depth). Furthermore, the cell is modular to allow for easier cleaning as TLFs are very susceptible to contamination and dust particles.

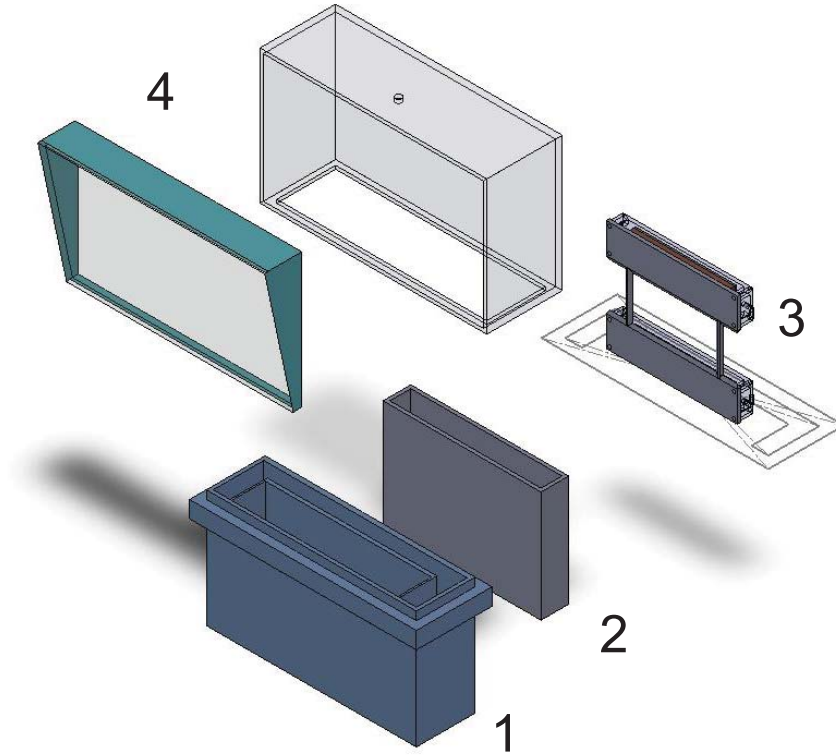


Figure 3: Assembly explosion rendering,(1) container, (2) solution reservoir, (3) frame assembly, (4) top enclosure

C. Frame Assembly

The frame is a modular assembly of four edge elements and two temperature control units, which can be mounted at the top and bottom. The edges which are holding the thin liquid film are sharply angled to allow a formation of the thin liquid film at the center position. Figure 5 shows the position of the frame inside the measuring chamber with the attached temperature control device at the top and at the bottom and figure 4 displays an explosion rendering of these devices. The base aluminum plate (1) is heated or cooled by an array of thermo-electric couplers (TEC) (2) which in turn are cooled by a separate closed water cooling loop via the copper cooling block (3). The assembly is then closed with a top cover (4) and a sealing to make it waterproof. Cabling and the outlets of the water cooling loop exit through sealed tubes at the top of the temperature control units. To vary the aspect ratio of the TLF the vertical frame elements can be continuously shifted along the horizontal frame elements. The height of the frame can be adjusted inserting vertical frame elements of different length. Figure 4 displays an explosion

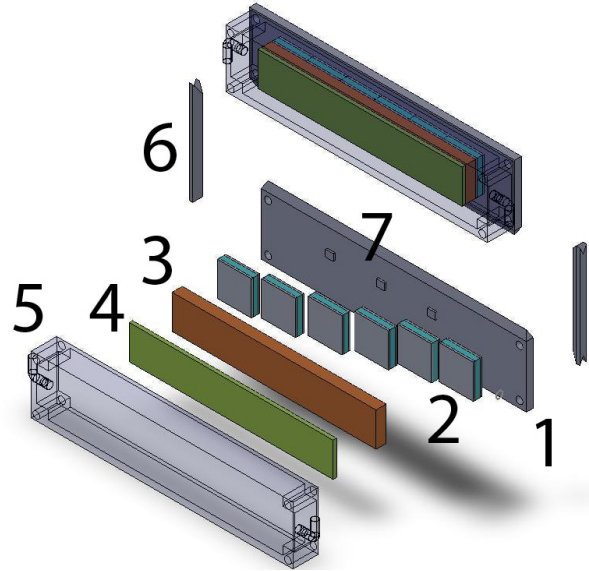


Figure 4: frame assembly explosion view. (1) aluminum base plate, (2) thermo-electric couplers array, (3) water cooling block, (4) insulation mat, (5) top cover, (6) adjustable vertical frame parts, (7) temperature sensors.

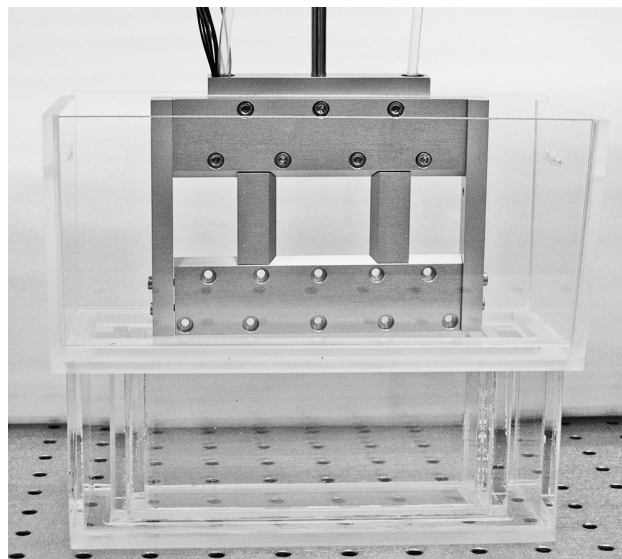


Figure 5: frame inside the measuring chamber - front view.

rendering of the frame assembly

III. EXPERIMENTAL DETAILS

A. Thin Film Generation

Macroscopic foam films are obtained by spanning an aluminum frame with surfactant solution, creating a quasi two-dimensional planar liquid. To create a TLF the frame assembly is submerged into the solution reservoir and by pulling the frame out liquid gets trapped between the edges of the frame, much like creating a soap bubble. The frame motion is controlled by a stepper motor which enables jerk-free motion to avoid any shock to the frame assembly which could cause the film to rupture. The speed of this process determines the initial thickness of the thin liquid film. The film then forms a wedge-like profile due to gravity. After the initial draining phase of excess fluid the gravitationally driven thinning process is orders of magnitude slower than the fluid transport by heat convection. Essentially, this enables us to keep the amount of liquid inside the frame constant as the liquid is transported as no drainage over the bottom meniscus occurs. Any loss in fluid volume can be attributed to the evaporation at the bottom heating element due to the lower concentration of water in the air.

The amount of fluid in the frame can be estimated by the number of visible stripe patterns of the captured reflection image. Details concerning the data acquisition are discussed in section IV.

B. System Control

The overall sensory input and control circuits are sketched in figure 6. The main components are the temperature input and analog voltage output which are managed by the LabVIEW application. For the most part there exist two temperature control schemes in research and industry: either the device is connected to a large thermal mass whose temperature is regulated by a flow-through cooler or a heat pump in form of a thermoelectric cooler (TEC) is employed. The type of device implemented depends on the scale of the setup, the expected temperature variation and the desired speed of temperature changes (dT/s). The dimensions of our setup are relatively small and the thermal mass of the frame elements is low which favours a temperature control setup based on TEC units which operate on a high update frequency to insure optimal temperature balance. Additionally, this enables us to quickly change the temperature with a controlled ramp up.

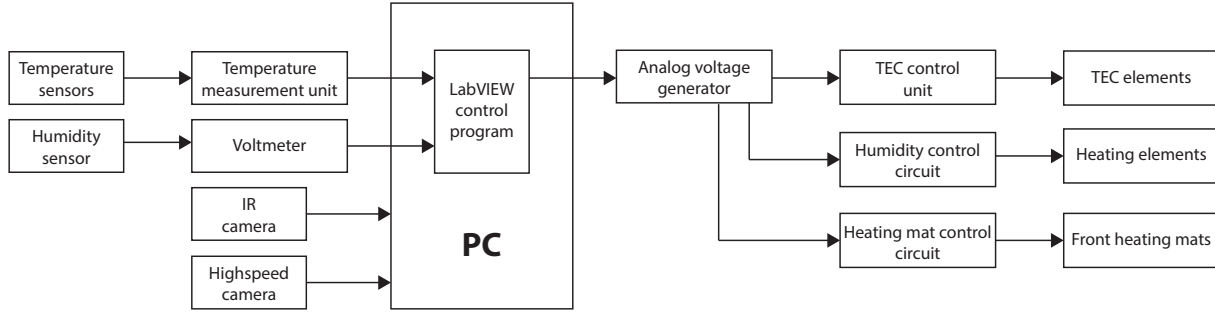


Figure 6: Schematic of the overall setup control

The TEC-arrays in the top and bottom frame unit are connected to a control unit which adjusts the amount of current flowing through the array to achieve a precisely controlled temperature. The bottom temperature control unit contains 6 TEC modules and the top unit contains 5 modules. Each module covers an area of 1 cm^2 and can pump a maximum of $Q_c = 5 \text{ W}$ allowing rapid temperature changes. The generated excess energy is dissipated by the water-cooled copper cooling blocks, which are connected to a large external heat exchanger. The wiring allows to control each TEC element individually to achieve better homogeneity of the temperature profile. In the current setup the elements for each section are wired in series and monitored by 4 temperature sensors.

The PID control loop for top and bottom temperature and humidity are realized in LabView together with the motor control for the automated frame submersion into the solution reservoir. The necessary wires and tubing for the water cooling loop exit the measurement chamber through holes in the side walls.

Temperature gradients up to $\Delta T = 40 \text{ K}$ are possible. The maximum temperature difference is limited by decreased film stability at high temperatures and increased condensation at the top border of the frame at temperatures close to the freezing point of the solution.

The humidity in the chamber is controlled by evaporating water from the water reservoir using two heating cartridges. Ideally, the concentration of water in the air inside the chamber is close to the dew point for the respective ambient temperature to avoid any evaporation from the TLF. To prevent the generated water vapor to condense on the observation window an array of heating mats is used. This system can also be used to adjust the ambient temperature inside the cell.

C. Surfactant Solution

The base solvent is deionized water, as it reduces contaminations with non-conducting carbon chain remnants or residual ion concentrations³⁰.

Glycerin is also required to achieve macroscopically large films with an area of several square centimeters or meters by adjusting the bulk viscosity^{7,43}. Due to its high viscosity ($\eta = 945 \text{ mPa}\cdot\text{s}^{-1}$, compared to $\sim 1 \text{ mPa}\cdot\text{s}^{-1}$ for water) it reduces the thinning speed of vertical films and allows the film to remain stable for a longer period of time⁵⁵. Typically, a concentration of 25 %_{vol} is used, yielding a net viscosity of $\sim 2 \text{ mPa}\cdot\text{s}^{-1}$, cf.⁵⁶.

The electrolyte concentration has a major effect on film stability and thickness⁵⁷. The addition of ions shields the electrostatic double-layer repulsion as described by the DLVO (Derjaguin-Landau-Verwey-Overbeek) theory¹⁵ hence permitting the appearance of a black film. Here, sodium chloride was chosen, since it has negligible influence on surface tension and critical micelle concentration (CMC). To eliminate any surface active contaminations, the laboratory grade *NaCl* was roasted at 600 °C.

The chosen surfactant, n-dodecyl- β -maltoside (β - $C_{12}G_2$), belongs to a new generation of sugar-based surfactants which are non-toxic, biodegradable and of low cost. β - $C_{12}G_2$ is a non-ionic surfactant which consists of hydrophilic head group, made up of two glucose rings ($C_6H_{12}O_6$) connected by an ether bond, and a hydrophobic alkyl chain ($C_{12}H_{25}$). The surfactant is soluble in water so that the hydrophilic head group is submerged in the core liquid. The hydrophobic tail is oriented normal to the liquid-air-interface and is not in contact with film surface. All experiments were performed with a concentration above the CMC, to guarantee that the equilibrium surface tension remains constant. Above CMC, deviations in surface surfactant density are compensated by diffusion of surfactants from or to the bulk liquid.

IV. DATA ACQUISITION AND PROCESSING

A non-invasive technique, Color Imaging Velocimetry (CIV), is used to capture and analyze the turbulent motion^{58,59}. In classic PIV (particle imaging velocimetry) applications small particles are seeded and traced to calculate flow properties. This technique has been previously employed in the study of soap films^{47,60,61}. However, for our setup the use of conventional PIV particles is not possible due to the fragility of the film and the feedback of the particles on the

flow: the film thickness one can still observe with CIV using visible light lies at $0.1\ \mu\text{m}$ to $2\ \mu\text{m}$ whereas the particles have a radius of $0.1\ \mu\text{m}$ to $5\ \mu\text{m}$.

A. Color Imaging Velocimetry

CIV is based on the thickness mapping of the TLF by capturing the reflection of a diffuse light from the surface^{62,63}. The interference pattern can be recorded monochromatically or in full color⁶⁴⁻⁶⁶. It is mostly used as a relative measure of the thickness distribution or an immediately available visualization of the flow structures. In order to get quantitative results a careful design is needed⁶⁷.

The interference of incident and reflected light yields a striped pattern, which can be used to infer the film thickness. Each color cycle corresponds to the multiples n of the smallest negative interference condition $(2 \cdot n + 1)\lambda\eta = 4h \cos \Theta$, where the refraction index, η , is assumed to be temperature-independent; Θ is the angle of incidence⁶².

The film is illuminated through this viewing window by an array of high power white LEDs which are placed behind a diffuser. Additionally, to avoid direct reflections of the light source from the viewing window, the front observation window is tilted downwards with respect to the liquid film plane.

The diffused light is reflected by the front and back side of the film whereas the front reflection is shifted by $\pi/2$ due to reflecting of an optically thicker medium. If the film thickness is much smaller than $\lambda/4$ of the smallest emitted wavelength the light waves interfere $\pi/2$ out-of-phase and no light is reflected. Hence the name black film although more precisely it is transparent. The reason why there is no smooth transition in the intensity of the reflected light is the abrupt change in thickness when the black film is formed. At $\lambda/4$ of the smallest wavelength, which is blue ($\sim 450\ \text{nm}$) in the case of the used white LEDs, the reflected waves interfere constructively. In addition, every other wavelength is reflected as well which sums up to a white color with a blue tint. Before that thickness is reached the film exhibits an orange tint as the film is approximately $200\ \text{nm}$ thick which corresponds to the cancellation of blue light, cf. figure 7(a). With this information the recorded color translates into a thickness profile of the TLF 7(c) To get an absolute value of the thickness corresponding to a certain color displayed one needs to take into account that the refractive index of the solution is slightly higher than that of pure water. At the end of this section, we would like to note that for Newton Black film, the film is

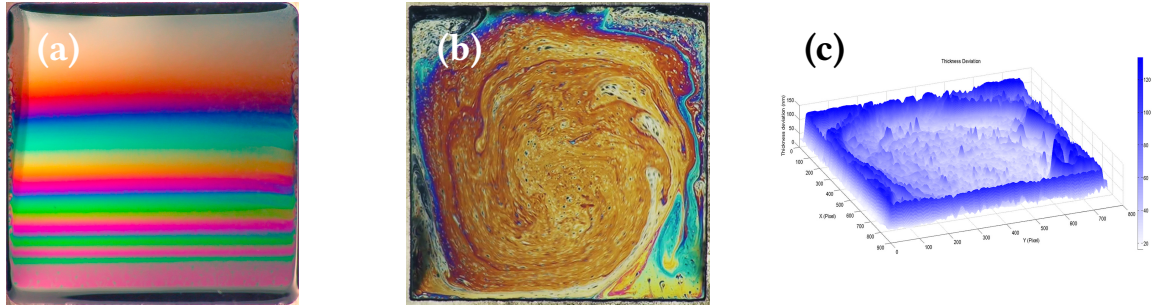


Figure 7: Snapshots and thickness profile of the TLF. (a): Stratified TLF with no temperature gradient applied. (b): Fully developed large scale circulation in a TLF. (c): Thickness deviation profile obtained by color analysis (spatial unit: Pixels).

transparent and CIV with visible light is not useable.

B. Data Acquisition and Processing

The reflected light is recorded with a high-speed camera at 500 frames per second with a resolution of 1.3 MPixel. As the reflected light cannot be captured at a 90° angle of incident, a Tilt-and-Shift lens is used which allows to tilt the focal plane to be parallel to the thin liquid film. The captured video data are filtered and converted into a binary image to analyze the behavior of domains of the same thickness.

Subsequently, in each frame, all clusters of the same thickness are numbered and consecutively linked through the following video frames. This enables us to track the volume, velocity, deformation rate and angular velocity of the moving fluid filaments. For each cluster the velocity is calculated using the shift of its center of mass per frame. The deformation rate is given by the scaling of the principal components. Similarly the angular velocity is given by the rotation of the principal component. Time-averaging over all frames then delivers the spatial characteristics of the flow field.

C. IR Imaging

The temperature distribution of the thin liquid film is measured non-invasively with the uncooled microbolometer-focal-plane-array IR Camera InfraTec®VarioCAM hr 680. The key specifications are the resolution of 640x480 Pixel, a capture frequency of up to 60 Hz, temperature

resolution of up to 0.03 K and a spectral range of 7.5 mm to 14 mm.

Infrared imaging of liquid thin films is non-trivial, as the radiation intensity emitted from the film is very low relative to the background noise. A non-uniform thickness can distort the measurement⁶⁸. Previously, infrared imaging was used to gather information about the instantaneous thickness profile and fluctuations of *strongly stratified* thin liquid films^{69,70}. To obtain the actual temperature distribution inside the film it is necessary to achieve a uniform thickness. In contrast to a stratified system the turbulence in our system is vigorous enough to break the stratification and involve the whole thin film in the convective motion. This enables a more homogeneous thickness throughout the film which makes it possible to retain temperature information without differing thermal emissivity due to large variations in thickness. As the IR-window is built into the back of the measurement chamber one can simultaneously observe the thin liquid film optically via the front window. Thus the infrared image can be synched to the reflective image and compensated by the thickness profile obtained from CIV to only retain temperature information. Result measurement using this method are work in progress and subject to future research.

V. TEMPERATURE STABILITY

In this section we will summarize the measured characteristics of the setup. A general overview of the temperature distribution in the frame is given by the infrared image of the frame assembly in figure 8. We define the temperature variation ΔT_V as the deviation from the set temperature along a line profile at the inner edges of the frame elements. The line profiles were measured at 5 s intervals for 30 minutes using the infrared camera, cf. Fig. 9. The setup was left to equilibrate for 20 minutes prior to the start of the measurement. The acquired temperature profiles were averaged for different temperature gradients ΔT and show a maximum temperature variation of $\Delta T_{V,max} = 1.5$ K. This may seem rather high in comparison to existing, larger volume Rayleigh-Bénard cells. However, previously published experimental designs aimed at thermal convection in thin liquid films do not elaborate on the temperature variation at all^{26,27,71}. The main difficulty in achieving a lower ΔT_V is the low thermal mass of the frame elements and the control of the TEC elements as a single array. For frame width of 20 mm and below we achieve a temperature variation of $\Delta T_V = 0.2$ K.

We define the temperature fluctuation δT as the variation from the line profile which has

been adjusted for its temporal average. We are able to control the average temperature control the average temperature fluctuation within $\langle \delta T \rangle = 0.05$ K. The temperature fluctuation of the maximum, minimum and mean temperature over time is shown in figure 10. Additional asymmetry of the temperature curves stems from the surface contact of the heating elements as the surface pressure varies slightly. The measured maximum heating temperature of the bottom segment is $T_{bot,max} = 55$ °C and the minimum temperature of the top element is achievable $T_{top,min} = 15$ °C with the bottom element at $T_{bot,max}$.

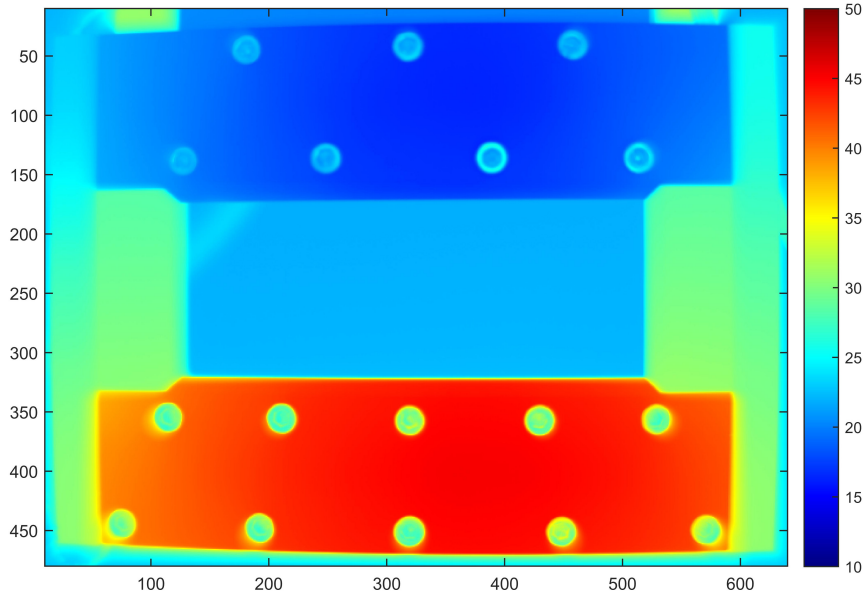


Figure 8: Infrared snapshot of the frame assembly at equilibrium temperature setpoint:

$$T_{top} = 18 \text{ } ^\circ\text{C}, T_{bot} = 43 \text{ } ^\circ\text{C}. \text{ Spatial unit: pixels, temperature in } ^\circ\text{C}$$

VI. SUMMARY AND OUTLOOK

A new apparatus for experiments on 2D convection has been developed, using thin liquid films. It consists of a fully transparent, sealable measurement chamber and a variable frame assembly. The principle application of the setup lies in the determination of the statistics of reversals in Rayleigh-Bénard convection, where the aspect ratio Γ can be effortlessly varied over a wide range. It thus allows the analysis of large scale convection reversals with varying geometry. The setup combines know-how from equilibrium state TLF experiments and classic Rayleigh-Bénard cells. The nonintrusive measurement technique CIV is applied to the system for measuring velocity profiles through the front observation window. The parameter space

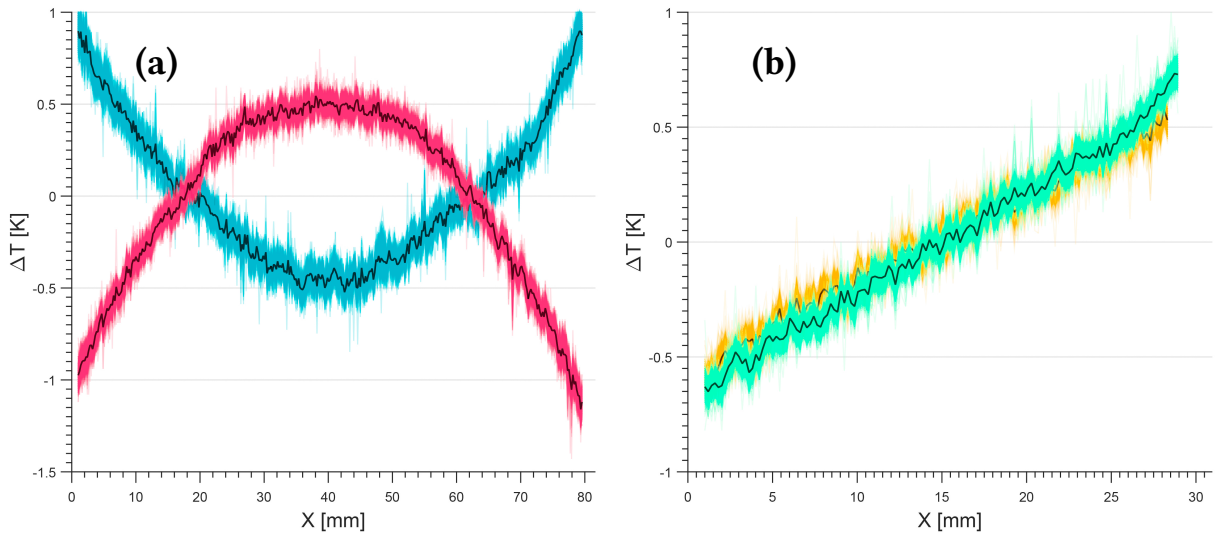


Figure 9: Temperature profiles of frame elements. Black line represents the average. (a): Top element (blue, cooling), and bottom element (red, heating). Variation of the heating element is higher due to the increased temperature difference with the surrounding atmosphere. (b): Vertical frame elements (left and right). Minimal variations in the profile occur due to the slight asymmetry of the bottom and top heating elements.

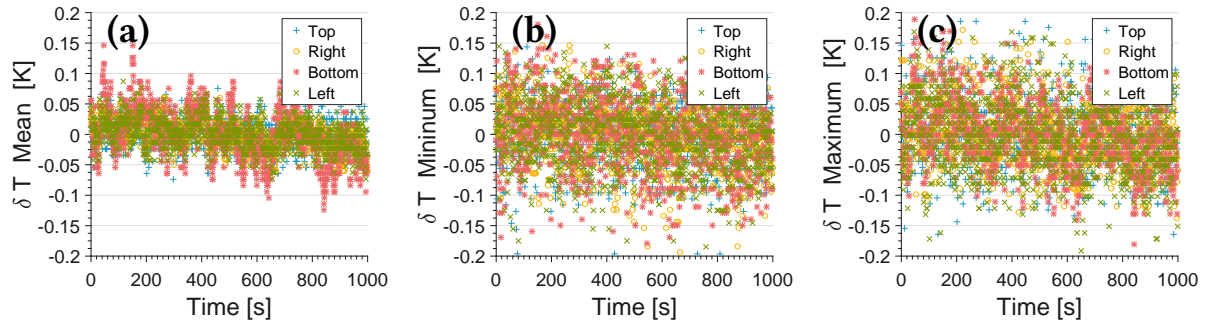


Figure 10: Fluctuation of the (a) mean, (b) minimum and (c) maximum temperature over time for each frame element.

for turbulent TLF experiments has been extended due to the large aspect ratio variation and temperature range.

As mentioned above, reversals in thin liquid films have an increased turn over period compared to classic Rayleigh-Bénard setups. Therefore, it is possible to gather reliable statistics in a shorter amount of time or increase the accuracy with longer observation times. Results will be published elsewhere.

Another frontier in TLF convection experiments is the measurement of convection in the equilibrium phase (NBF or CBF), as no visible light is reflected from these films. Currently, the only way to get information on the velocity field is through residual domains of thicker film which are advected and act as tracers. Any PIV technique is even more out of the question at film thicknesses below 50 nm. Two viable options exist to image motion in black films, which will be explored: If the film is in the meta-stable Common black film phase, the use of commercially available fluorescent particles⁷² may be possible. Otherwise fluorescent molecules like manufactured liposomes are an option⁷³.

We conclude that we have presented a dedicated device for the measurement of reversals in Rayleigh/Bénard convection. Beyond this very specific use, general experiments for 2D liquids can be performed, we consider, however, the perspective for measurements on nonequilibrium thin-films as very promising, too. Controlled measurements in this direction are very complicated, and we have built a well-designed setup where all relevant thermodynamic quantities can be controlled, including chemistry.

REFERENCES

- ¹G. Ahlers, S. Grossmann, and D. Lohse. Heat transfer and large scale dynamics in turbulent Rayleigh-Bénard convection. *Reviews of Modern Physics*, 81:503–537, April 2009.
- ²D. Lohse and K.-Q. Xia. Small-Scale Properties of Turbulent Rayleigh-Bénard Convection. *Annual Review of Fluid Mechanics*, 42:335–364, January 2010.
- ³Kazuyasu Sugiyama, Rui Ni, R.J.A.M. Stevens, T. S.Chan, S.-Q. Zhou, H.-D. Xi, C. Sun, S. Grossmann, K.-Q. Xia, and D. Lohse. Flow reversals in thermally driven turbulence. *Phys. Rev. Lett.*, 105:034503–1–4, 2010.
- ⁴Pankaj Kumar Mishra, AK De, MK Verma, and V Eswaran. Dynamics of reorientations and reversals of large-scale flow in rayleigh-bénard convection. *Journal of Fluid Mechanics*, 668:480–499, 2011.
- ⁵François Pétrélis, Stéphan Fauve, Emmanuel Dormy, and Jean-Pierre Valet. Simple mechanism for reversals of earth’s magnetic field. *Phys. Rev. Lett.*, 102(14):144503, 4 2009.
- ⁶Francisco Fontenele Araujo, Siegfried Grossmann, and Detlef Lohse. Wind reversals in turbulent rayleigh-bénard convection. *Physical review letters*, 95(8):084502, 2005.
- ⁷B. K. Martin, X-L. Wu, W. I. Goldburg, and M. A. Rutgers. Spectra of decaying turbulence in a

- soap film. *Phys. Rev. Lett.*, 80(18):3964–3967, 1998.
- ⁸J. Zhang, XL Wu, and K.Q. Xia. Density fluctuations in strongly stratified two-dimensional turbulence. *Physical review letters*, 94(17):174503, 2005.
- ⁹F. Seychelles, F. Ingremeau, C. Pradere, and H. Kellay. From intermittent to nonintermittent behavior in two dimensional thermal convection in a soap bubble. *Physical review letters*, 105(26):264502, 2010.
- ¹⁰D. Exerowa and P.M. Kruglyakov. *Foam and foam films: theory, experiment, application*. Elsevier, New York, 1998.
- ¹¹IB Ivanov. *Thin liquid films: fundamentals and applications*, volume 29 of *surfactant science series*. Marcel Dekker, Inc., 1988.
- ¹²Naveen Tiwari, Zoltan Mester, and Jeffrey M. Davis. Stability and transient dynamics of thin liquid films flowing over locally heated surfaces. *Phys. Rev. E*, 76(5):056306, 11 2007.
- ¹³C. Stubenrauch and R. Miller. Stability of foam films and surface rheology: an oscillating bubble study at low frequencies. *The Journal of Physical Chemistry B*, 108(20):6412–6421, 2004.
- ¹⁴V. Bergeron. Forces and structure in thin liquid soap films. *Journal of Physics: Condensed Matter*, 11:R215, 1999.
- ¹⁵B.V. Derjaguin. *Theory of stability of colloids and thin films*. Consultants Bureau New York and London, 1989.
- ¹⁶G. Reiter. The artistic side of intermolecular forces. *Science*, 282(5390):888, 1998.
- ¹⁷H. Kellay. Turbulence: Thick puddle made thin. *Nature Physics*, 7(4):279–280, 2011.
- ¹⁸P.J. Yunker, T. Still, M.A. Lohr, and AG Yodh. Suppression of the coffee-ring effect by shape-dependent capillary interactions. *Nature*, 476(7360):308–311, 2011.
- ¹⁹S. Davey. Enantiomer separation: Selective soap-films. *Nature Chemistry*, 2010.
- ²⁰Eds. Prud’homme R. K., Khan S. A. *Foams: Theory, Measurements, and Applications*. Dekker, N.Y., 1996.
- ²¹J. Vermant. Fluid mechanics: When shape matters. *Nature*, 476(7360):286–287, 2011.
- ²²E. J. W. Verwey and J. T. G. Overbeek. *The Theory of the Stability of Lipophobic Colloids*. Elsevier, Amsterdam, 1948.
- ²³M.N. Jones, K.J. Mysels, and P.C. Scholten. Stability and some properties of the second black film. *Transactions of the Faraday Society*, 62:1336–1348, 1966.
- ²⁴J.N. Israelachvili. *Intermolecular and surface forces*. Academic press London, 1991.
- ²⁵I. B. Ivanov. Foams: Theory, measurements, and applications. *Pure Appl. Chem.*, 52:1241–1262,

- 1980.
- ²⁶J. Zhang and XL Wu. Velocity intermittency in a buoyancy subrange in a two-dimensional soap film convection experiment. *Physical review letters*, 94(23):234501, 2005.
- ²⁷F. Seychelles, Y. Amarouchene, M. Bessafi, and H. Kellay. Thermal Convection and Emergence of Isolated Vortices in Soap Bubbles. *Phys. Rev. Lett.*, 100(14):144501, 2008.
- ²⁸CJW Breward and PD Howell. The drainage of a foam lamella. *Journal of Fluid Mechanics*, 458:379–406, 2002.
- ²⁹PD Howell and HA Stone. On the absence of marginal pinching in thin free films. *European Journal of Applied Mathematics*, 16(5):569–582, 2005.
- ³⁰RM Muruganathan, R Krustev, H-J Müller, H Möhwald, B Kolaric, and R v Klitzing. Foam films stabilized by dodecyl maltoside. 1. Film thickness and free energy of film formation. *Langmuir: the ACS journal of surfaces and colloids*, 20(15):6352, 2004.
- ³¹A. Thess, F. Busse, R. Du Puits, C. Resagk, and A. Tilgner. The barrel of ilmenau: a novel facility for experiments on high rayleigh number convection. In *APS Division of Fluid Dynamics Meeting Abstracts*, volume 1, 2001.
- ³²Ronald du Puits, Christian Resagk, and André Thess. Breakdown of wind in turbulent thermal convection. *Phys. Rev. E*, 75(1):016302, 1 2007.
- ³³C. Resagk, R. Du Puits, A. Thess, F.V. Dolzhansky, S. Grossmann, F.F. Araujo, and D. Lohse. Oscillations of the large scale wind in turbulent thermal convection. *Physics of Fluids*, 18:095105, 2006.
- ³⁴Francisco Fontenele Araujo, Siegfried Grossmann, and Detlef Lohse. Wind reversals in turbulent rayleigh-bénard convection. *Phys. Rev. Lett.*, 95(8):084502, 8 2005.
- ³⁵L. Bureau. Nonlinear Rheology of a Nanoconfined Simple Fluid. *Physical Review Letters*, 104(21):218302, May 2010.
- ³⁶R. J. A. M. Stevens, J.-Q. Zhong, H. J. H. Clercx, G. Ahlers, and D. Lohse. Transitions between Turbulent States in Rotating Rayleigh-Bénard Convection. *Physical Review Letters*, 103(2):024503, July 2009.
- ³⁷Takatoshi Yanagisawa, Yasuko Yamagishi, Yozo Hamano, Yuji Tasaka, and Yasushi Takeda. Spontaneous flow reversals in rayleigh-bénard convection of a liquid metal. *Phys. Rev. E*, 83(3):036307, 3 2011.
- ³⁸P. K. MISHRA, A. K. DE, M. K. VERMA, and V. ESWARAN. Dynamics of reorientations and reversals of large-scale flow in rayleigh-bénard convection. *Journal of Fluid Mechanics*, 668:480–

- 499, 2011.
- ³⁹K.J. Mysels, S. Frankel, and K. Shinoda. *Soap films: studies of their thinning and a bibliography*. Pergamon Press, 1959.
- ⁴⁰Y. Couder, J.M. Chomaz, and M. Rabaud. On the hydrodynamics of soap films. *Physica D*, 37(1-3):384–405, 1989.
- ⁴¹J.M. Chomaz. The dynamics of a viscous soap film with soluble surfactant. *Journal of Fluid Mechanics*, 442:387–409, 2001.
- ⁴²R. Bruinsma. Theory of hydrodynamic convection in soap films. *Physica A Statistical Mechanics and its Applications*, 216:59–76, 1995.
- ⁴³H. Kellay, X-L Wu, and W. I. Goldburg. Experiments with turbulent soap films. *Phys. Rev. Lett.*, 74(20):3975–3978, 1995.
- ⁴⁴U. Frisch. *Turbulence: The legacy of A. N. Kolmogorov*. Cambridge Univ. Press, Cambridge, UK, 1995.
- ⁴⁵H. Kellay. Dispersion in the enstrophy cascade of two-dimensional decaying grid turbulence. *Physical Review E*, 69(3):36305, 2004.
- ⁴⁶M.C. Jullien, J. Paret, and P. Tabeling. Richardson pair dispersion in two-dimensional turbulence. *Physical review letters*, 82(14):2872–2875, 1999.
- ⁴⁷P. Vorobieff, M. Rivera, and RE Ecke. Soap film flows: Statistics of two-dimensional turbulence. *Physics of Fluids*, 11:2167, 1999.
- ⁴⁸M. Rivera, P. Vorobieff, and R.E. Ecke. Turbulence in flowing soap films: Velocity, vorticity, and thickness fields. *Phys. Rev. Lett.*, 81(7):1417–1420, 1998.
- ⁴⁹T. Shakeel and P. Vorobieff. Decaying turbulence in soap films: energy and enstrophy evolution. *Experiments in Fluids*, 43(1):125–133, 2007.
- ⁵⁰T. Schnipper, A. Andersen, and T. Bohr. Vortex wakes of a flapping foil. *Journal of Fluid Mechanics*, 633:411–423, 2009.
- ⁵¹Albert van den Berg, Harold G Craighead, and Peidong Yang. From microfluidic applications to nanofluidic phenomena. *Chem. Soc. Rev.*, 39(3):899–1220, 2010.
- ⁵²Subhalakshmi Kumar Steve Granick, Sung Chul Bae and Changqian Yu. Confined liquid controversies near closure? *Physics*, 3:73, 8 2010.
- ⁵³Lyderic Bocquet and Elisabeth Charlaix. Nanofluidics, from bulk to interfaces. *Chem. Soc. Rev.*, 39(3):1073–1095, 2010.
- ⁵⁴Shah H. Khan, George Matei, Shivprasad Patil, and Peter M. Hoffmann. Dynamic solidification

- in nanoconfined water films. *Phys. Rev. Lett.*, 105(10):106101, 8 2010.
- ⁵⁵C. Isenberg. *The science of soap films and soap bubbles*. Dover Pubns, 1992.
- ⁵⁶MA Rutgers, XL Wu, and WB Daniel. Conducting fluid dynamics experiments with vertically falling soap films. *Review of Scientific Instruments*, 72:3025, 2001.
- ⁵⁷L. Zhang, P. Somasundaran, and C. Maltesh. Electrolyte Effects on the Surface Tension and Micellization of n-Dodecyl- β -d-Maltoside Solutions. *Langmuir*, 12(10):2371–2373, 1996.
- ⁵⁸M. Winkler and M. Abel. Mixing in thermal convection of very thin free-standing films. *Physica Scripta Volume T*, 155(1):014020, July 2013.
- ⁵⁹M. Winkler, G. Kofod, R. Krastev, S. Stöckle, and M. Abel. Exponentially fast thinning of nanoscale films by turbulent mixing. *Physical Review Letters*, 110(9):094501, March 2013.
- ⁶⁰C. Cheung, YH Hwang, X. Wu, and HJ Choi. Diffusion of particles in free-standing liquid films. *Physical review letters*, 76(14):2531–2534, 1996.
- ⁶¹P. Vorobieff, M. Rivera, and R.E. Ecke. Imaging 2D turbulence. *Journal of Visualization*, 3(4):323–330, 2001.
- ⁶²L.J. Atkins and R.C. Elliott. Investigating thin film interference with a digital camera. *American Journal of Physics*, 78:1248, 2010.
- ⁶³J.G.H. Joosten. *Light Scattering from thin liquid films*, volume 29 of *surfactant science series*. Marcel Dekker, Inc., 1988.
- ⁶⁴HM Princen and SG Mason. Optical interference in curved soap films. *Journal of colloid science*, 20(5):453–463, 1965.
- ⁶⁵M. Gharib and M. Beizaie. Visualization of two-dimensional flows by a liquid (soap) film tunnel. *Journal of visualization*, 2(2):119–126, 1999.
- ⁶⁶T.S. Yang, C.Y. Wen, and C.Y. Lin. Interpretation of color fringes in flowing soap films. *Experimental Thermal and Fluid Science*, 25(3-4):141–149, 2001.
- ⁶⁷M. Winkler and M. Abel. Droplet coalescence in 2d thermal convection of a thin film. *Journal of Physics Conference Series*, 333(1):012018, December 2011.
- ⁶⁸W. Minkina and S. Dudzik. *Infrared Thermography*. Wiley Online Library, 2009.
- ⁶⁹J. Zhang, XL Wu, and N. Rashidnia. Thermal radiation and thickness fluctuations in freely suspended liquid films. *Physics of Fluids*, 18:085110, 2006.
- ⁷⁰J. Zhang and XL Wu. Persistent skewness of a strongly active scalar. *Physical Review E*, 79(4):045301, 2009.
- ⁷¹B. Martin and X-L. Wu. Double-diffusive convection in freely suspended soap films. *Phys. Rev.*

Lett., 80(9):1892–1895, 1998.

⁷²TSI. Seed particles fluorescent particles 10 nm 540-560nm 10 ml. website, (<http://www.tsi.com/productView.aspx?id=24418>), 2012.

⁷³A.K. Singh, E.B. Cummings, and D.J. Throckmorton. Fluorescent liposome flow markers for microscale particle-image velocimetry. *Analytical chemistry*, 73(5):1057–1061, 2001.